Def Sci J, Vol 39, No. 4, October 1989, pp 411-423

Phonons in Semiconductor Superlattices

A.K. Sood

Department of Physics, Indian Institute of Science, Bangalore-560 012

ABSTRACT

This paper presents a review of the novel features of the vibrational properties of the semiconductor superlattices, as studied mostly by Raman scattering. The concepts of folding and confinement applicable to acoustic and optic phonons and the existence of interface phonons are brought out. The role of Raman scattering in characterising the structural quality of the superlattices is mentioned.

1. INTRODUCTION

Phonons in semiconductor superlattices (SLs) composed of alternate layers of two different semiconductors have a number of novel features as compared to those in the corresponding bulk semiconductors[1-3]. Their understanding is not only interesting in its own right, but can also be of considerable importance in the characterisation of the interface roughness[4,5] and broadening of interfaces due to heat-induced interdiffusion in the growth process[6,7]. The experimental technique which has been most effectively used is resonance Raman scattering. Raman scattering involves the coupling of light to phonons via the electronic system. Hence Raman experiments yield information on the electron-phonon interaction which is important in controlling the transport properties in superlattice devices. Furthermore, Raman measurements of the confined optical phonons in the SLS can be used to determine the phonon dispersion in the bulk material which is otherwise conventionally done by neutron scattering[8].

Phonons in an SL can be understood by the concept of folding or confinement, depending on whether the phonon branches of the two constituent materials overlap in frequency or not[1-3,8]. The acoustic phonon branches of the two semiconductors comprising the SL always overlap in frequency and hence the acoustic phonons can propogate normal to the interfaces, i.e., along the growth direction. The growth direction in most of the SLs is (001) (z-direction). The new features introduced due to additional periodicity of the SL are:

Received 21 July 1989

(a) folding of the average acoustic branch at the new Brillouin zone, π/d, and (b) opening of gaps at zone-centre and π/d, similar to formation of band gaps in the free-electron dispersion due to crystal potential. Here $d = d_1 + d_2$ where d_1 is the thickness of layer 1 (say *GaAs*) and d_2 is the thickness of layer 2 (say $Ga_{1-x}Al_xAs$) in *GaAs*-$Ga_{1-x}Al_x$ SL.

In contrast to the acoustic phonons, the optical phonon frequencies of the constituent materials may overlap in some region or may not overlap at all. In the former case, the optical phonons can be described by folding into the reduced Brillouin zone (0 to π/d), similar to the acoustic phonons. In the latter situation where the optical phonon branches in the two layers are separated in energy, as in *GaAs-AlAs* SL, the phonons can not propagate along the z-direction and hence are confined in each layer[8-10], analogous to electron or hole confinement in quantum wells. The confined phonons though dispersionless for wave vector along the superlattice growth direction (referred to as z-direction henceforth) have considerable dispersion parallel to x and y axes[11,12]. The presence of interfaces in the SL gives rise to optical (Fuchs-Kliewer-like) interface phonons[13-15] and acoustical (Lamb- and Love-like) guided phonons[12] for wave vectors parallel to the interface planes. The vibrational amplitude of these interface phonons decays exponentially away from the interface in z-direction and is non-zero in either layer. The latter aspect distinguishes them from the confined optical phonons where vibrational amplitude is localised only in one layer.

Most of the work on the vibrational as well as the electronic properties has been done on lattice-matched (001) grown *GaAs-AlGa As* SLs[1-3]. Recently, strained-layer SLs *GaSb-AlSb*[16,17], *Si-Ge*[18,19] and *ZnSe*-$Zn_{1-x}Mn_xSe$ have been studied by Raman scattering. Suh *et al.*[20] have also investigated SLs of *Mn*-based II-VI dilute magnetic semiconductors—$Cd_{1-x}Mn_xTe/Cd_{1-y}Mn_yTe$. Experiments have also been done[21] to study folded acoustic phonons in amorphous semiconductor SLs a-*Si/SiN*.

Section 2 of this paper deals with the folded acoustic phonons, covering both experimental results and theoretical models. The confined optical phonons are discussed in Section 3, with particular reference to our own work on *GaAs-AlAs* SLs. Section 4 covers the interface phonons. The available results on effect of the interface roughness on the phonons are summarised in Section 5.

2. FOLDED ACOUSTIC PHONONS

An umambigous demonstration of the folded longitudinal acoustic (LA) phonons in the semiconductor SL was given by Raman experiments on short period *GaAs-AlAs* SL[22]. The first evidence of gap formation at the minizone boundary π/d was provided by phonon transmission measurements using superconducting tunnel junctions[23]. Figure 1 shows Raman spectra of 42 Å *GaAs*-8 Å $Al_xGa_{1-x}As$ SL recorded in $z(xx)\bar{z}$ and $z(xy)\bar{z}$ scattering configurations. Here the symbols within (outside) the brackets indicate the radiation polarisation (wave vector) and $x\,||\,(100), y\,||\,(110)$ and $z\,||\,(001)$. The three doublets seen in $z(xx)\bar{z}$ scattering geometry near 30, 60 and 90 cm^{-1} are due to the folded LA modes which acquire Raman activity due to minizone folding. The basis for the assignment of the modes to the folded LA phonons comes from the calculated phonon dispersion curves.

2.1 Simple Theoretical Models

Two simple approaches can be taken to calculate the dispersion curves for the acoustic phonons. One approach given by Rytov[24] is based on elastic continuum model (ECM) in

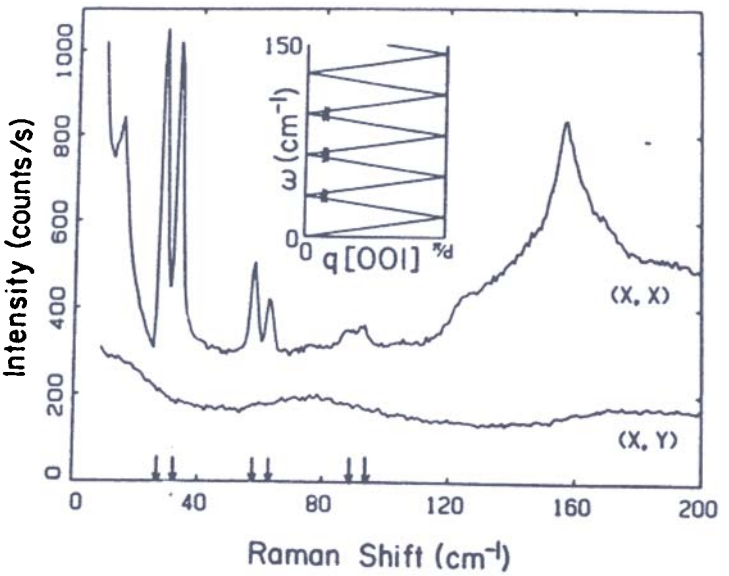

Figure 1. Raman spectra of 42 Å $GaAs$-8 Å $Al_{0.3}Ga_{0.7}As$ SL. Inset shows the calculated dispersion curve based on the ECM Eqn. (11) (after Ref. 10).

which each layer is treated as an elastic continum characterised by density ρ and sound velocity v. The dispersion relation for a periodic sequence of two layers with thickness d_1 (density ρ_1 and velocity v_1) and thickness d_2 (density ρ_2 and velocity v_2) is given by

$$\cos(qd) = \cos(k_1 d_1)\cos(k_2 d_2) - (1+\delta)\sin(k_1 d_1)\sin(k_2 d_2) \tag{1}$$

where $\delta = \dfrac{(1-K)^2}{2K}$, $K = \dfrac{\rho_2 v_2}{\rho_1 v_1}$ and $k_{1(2)} = \omega / v_{1(2)}$.

Here q is the wave vector along the z-direction. Equation (1) has been plotted as an inset in Fig. 1, with parameters appropriate for the SL. It can be seen from the inset that the experimentally observed values of the doublet (marked by solid points) agree well with the calculated dispersion curves. It may be remembered that in a scattering experiment, q is given by

$$q = \frac{4\pi n}{\lambda}\sin\left(\frac{\theta}{2}\right) \tag{2}$$

where n is the refractive index of the material, θ is the scattering angle and λ is the wavelength of incident laser light. By varying λ and θ, the dispersion curves can be scanned.

It can be seen that the presence of δ in Eqn. (1) introduces gaps in the dispersion curves at $q = 0$ and $q = \pi/d$. The magnitude of gaps is[25]

$$\Delta\omega = \frac{\delta\,\bar{v}}{d}\sin\left(\frac{m\,\pi\,d_1 v_2}{d_1 v_2 + d_2 v_1}\right) \tag{3}$$

where $\bar{v}$ is the average sound velocity,

$$\frac{1}{\bar{v}} = \frac{1}{d}\left(\frac{d_1}{v_1} + \frac{d_2}{v_2}\right)$$

The second approach for calculating the dispersion relations is based on the linear-chain model[26,10] (LCM) in which a single nearest neighbour spring constant is the only free parameter for longitudinal vibrations whereas two spring constants are required for

transverse vibrations. The ECM is not adequate if the acoustic phonon dispersions in the bulk constituent materials of the SL are not linear at high q. In such cases, one should use the LCM to analyse the folded phonons. An example of inadequacy of ECM is the case for *GaSb-AlSb* SL, as shown by Raman scattering results[16]. Figure 2 shows the dispersion curves in two models for 13.7 Å *GaSb*-13.7 Å *AlSb* SL. The crosses are the observed values of the folded LA mode frequencies (for more details, see ref. 16). It can be seen that the observed frequencies agree better with the LCM than with the ECM.

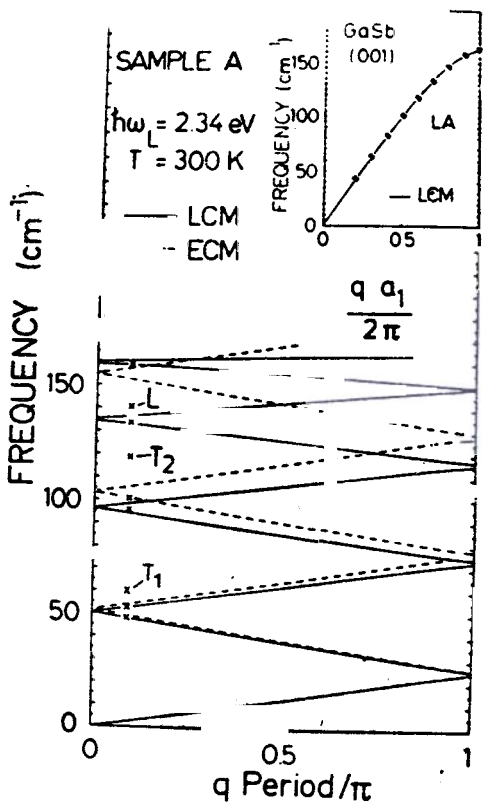

2. Comparison of the observed frequencies of the folded LA phonons in *GaSb-AlSb* SL with calculated dispersion curves based on ECM and LCM. The inset shows the LA phonon dispersion in bulk *GaSb*.

2.2 Symmetry

The LA phonons with $q = 0$ belong to the irreducible representations A_1 and B_2 of the point group symmetry D_{2d} of the SL grown along (001). The displacement field (strain) produced by B_2 phonons is symmetric (antisymmetric) and by A_1 phonons antisymmetric (symmetric) with respect to the centre of each layer. Hence only A_1 phonons (symmetric strain) will couple to light via the photoelastic mechanism[22] and will be seen in $z(xx)\bar{z}$ scattering geometry. At finite q as in a backscattering Raman experiment, both the A_1 and B_2 modes contain some admixture of the $q = 0$ A_1 mode[27], giving rise to doublets, as seen in Fig. 1.

In resonant Raman scattering when the incident or scattered photon energy is close to some electronic transition in a SL, the situation is quite complicated and not fully understood quantitatively. To illustrate it, we show our recent results[16] on 13.7 Å *GaSb*-13.7 Å. *AlSb* in Fig. 3. The spectra in Fig. 3(b) and 3(c) are under resonant conditions. The doublets $m = \pm 1$ and ± 2 are seen even in $z(yx)\bar{z}$ geometry which should show B_2 phonons. There are a number of other interesting features in resonant conditions[16].

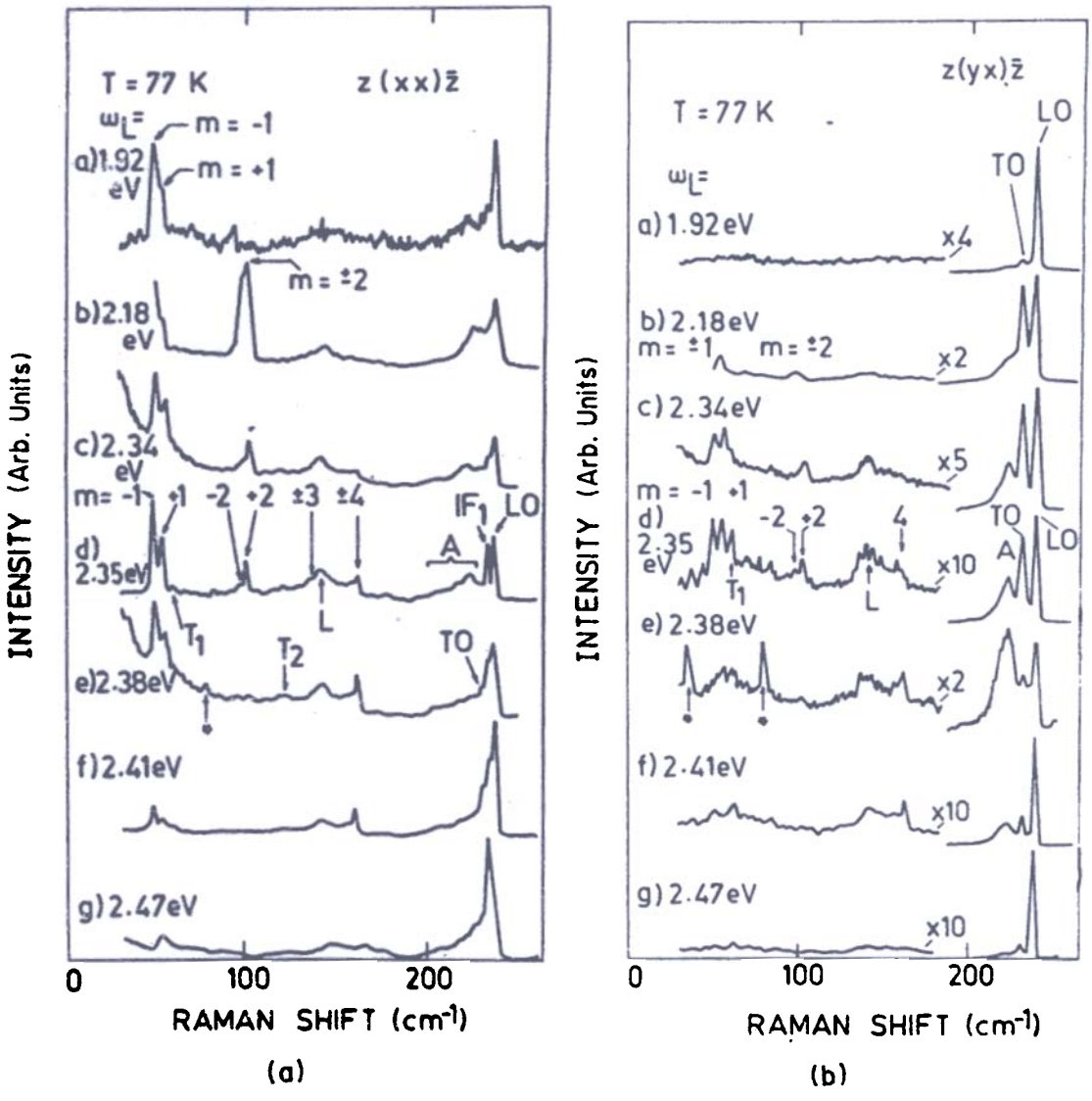

Figure 3. Raman spectra for 13.7 Å *GaSb*-13.7 Å *AlSb* SL: (a) $z(xx)\bar{z}$ configuration, (b) $z(yx)\bar{z}$ configuration.

It may be noted that for some frequency regions, the acoustic phonon branches of the two layer materials may not overlap and in that case, one should get confinement effect where the thickness of the layer d_1 (or d_2) and not the superlattice period d is relevant. An example of the confined acoustic phonon is provided by the calculation for *GaAs-AlAs* SL[12]. For the *TA* modes with the wave vector q_z, there is confinement to the *AlAs* layer higher (*AlAs*-like) frequencies.

3. OPTICAL PHONONS

For non-overlapping optical phonon branches of the SL, each layer acts as a 'phonon-quantum well' for optical phonons with wave vector along q_z. The magnitude of confinement has been quantified in the linear chain model[10], *ab-initio* calculations based on planar force constants[28], three-dimensional shell-model calculations[12] and 11-parameter rigin-ion-model incorporating long-range coulomb interactions[11]. The strength of confinement depends on the ratio of reduced masses and the force constants in the two layer materials. In *GaAs-AlAs* SL, the decay length of the *GaAs*-like *LO* phonon in the adjacent *AlAs* layer is about one monolayer (~ 2.83 Å) where the *AlAs*-like *LO* modes are even more confined (~ 1/3 monolayer). This is basically due to a very large difference in

the masses of the *Ga* atoms ($m = 70$ amu) and the *Al* atoms ($m = 27$ amu). Let us consider a specific example of the $(GaAs)_n$-$(AlAs)_1$ SL with n monolayers (monolayer thickness $a = 2.83$ Å) of *GaAs* and 1 monolayers of *AlAs* ($d_1 = na$, $d_2 = 1.a$). The displacement patterns of the atoms in the confined modes in either layer, say *GaAs*, can be written to a good approximation in the form of standing waves as[12,29,30].

$$u_z(m) \sim \cos(q_m z),\ m = 1, 3, 5, \ldots\ (B_2 \text{ modes})$$

and

$$u_z(m) \sim \sin(q_m z),\ m = 2, 4, 6, \ldots\ (A_1 \text{ modes}) \tag{4}$$

with an effective wave vector

$$q_m = \frac{m\pi}{\quad} \tag{5}$$

In Eqn. (4) the origin of z is taken at the centre of *GaAs* layer; m is an integer ranging from 1 to n. The displacement pattern of the mth confined mode has m half-wavelengths in the layer. The effective thickness of the layer appearing in q_m is $(n+1)a$, which is larger than the stoichiometric thickness d_1 ($=na$). This difference was pointed out[29] by realising that the interfacial *As* atoms have finite displacement and the first clamped atom is the first aluminium atom in the *AlAs* layer.

Let us see how these modes can be seen in Raman scattering. Figure 4 shows Raman spectra[8] of 20 Å *GaAs*-60 Å *AlAs* SL in the backscattering geometry for off-resonance (Fig 4(a)) and near resonance (Fig. 4(b)). The off-resonance spectra shows odd m-modes of B_2 symmetry in $z(xy)\bar{z}$ geometry and a weak $m = 2$ mode of A_1 symmetry in $z(xx)\bar{z}$ geometry.

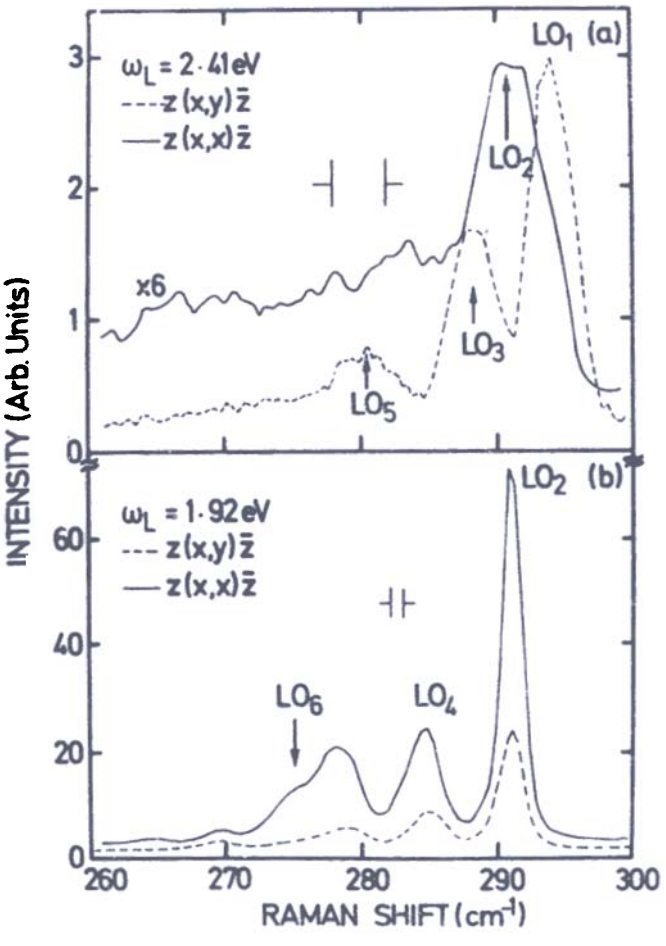

Figure 4. (a) Off-resonance spectra, (b) near resonance for 20 Å *GaAs*-60 Å *AlAs* SL (after Ref. 8.).

The scattering strength of A_1 mode is enormously enhanced in near-resonance conditions. In addition, the scattering is depolarised in resonance condition so as to give A_1 modes (even m) in $z(xy)\bar{z}$ geometry. This depolarisation scattering has been attributed to impurity-induced Fröhlich mechanism[8] which has been corroborated by recent resonance Raman studies of Grant *et al.* and Sela *et al*[31]. The dominance of A_1 phonons in resonance conditions has been understood on the basis of Frölich mechanism and symmetry properties of the confined modes[8]. Ishibashi *et al.*[32] have reported the Raman data of the LO_1 modes for the *GaAs*-like and *AlAs*-like phonons in $(GaAs)_n$ $(AlAs)_1$ ultrathin layer SLs $(1 \leq n, 1 \leq 6)$.

Figure 5 shows resonance Raman spectra from the same SL as in Fig. 4. A number of

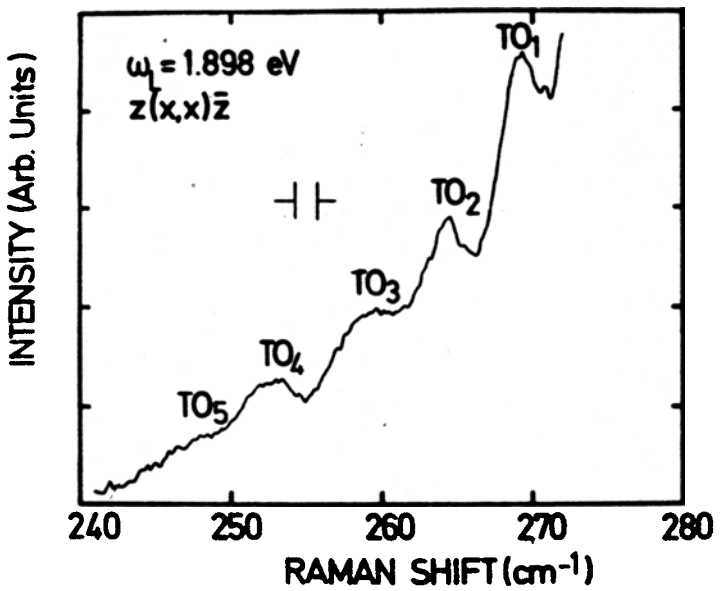

Figure 5. Confined *TO* modes recorded in near resonance spectrum of *GaAs-AlAs* SL (after Ref. 8).

peaks are observed which are attributed to the confined *TO* modes. The *TO*-phonons of the SL should not be seen in true backscattering geometry (since they belong to the *E*-representation). The breakdown of the selection rule may lie in the defect induced wavevector non-conservation scattering process.

The observed frequencies of the confined LO_m and TO_m modes can be used to map the dispersion curve $\omega(q)$ for bulk crystals (q along (001)) by identifying q with q_m given by Eqn. (5). Figure 6 shows the observed frequencies of LO_m and TO_m confined modes in *GaAs* layer for a number of *GaAs-AlAs* SLs. Also shown in Fig. 6 is the room temperature neutron scattering data[33] which has been displaced by 10 cm^{-1} to account for temperature shift and to match $q = 0$ Raman phonon frequency at 10 K. Dotted curves are the calculated dispersion curves for the bulk *GaAs*[34], based on the adiabatic bond-charge model. We notice from Fig. 6 that a discrepancy exists between the confined mode freuqencies for higher m and the bulk phonon dispersion. A similar difference was observed by other workers[35]. Recently, it has been shown that the above discrepancy can be due to interface roughness[5]. The confined phonons in the SLs grown by migration-enhanced epitaxy and molecular beam epitaxy with growth interruption, which favour the smoothness of interfaces, lie close to the recent low temperature neutron scattering results for the *LO*-phonon dispersion in bulk *GaAs*[5]. It has been pointed out that the higher order confined phonons are considerably more sensitive to the interface roughness than the low-order ones. This can be easily seen as follows. If the well thickness is changed by one

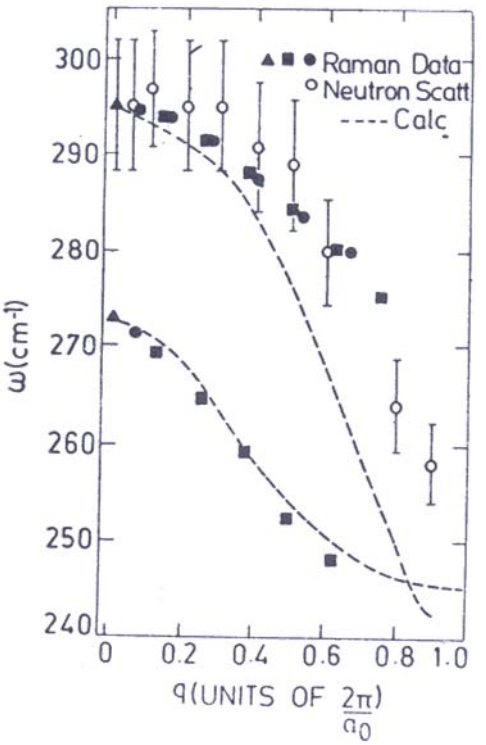

Figure 6. Observed LO_m and TO_m frequencies versus q_m given by Eqn. (5).

monolayer from n to $n \pm 1$, the change in the confinement wavevector q_m of the mth order phonon is (from Eqn. (5))

$$\frac{\Delta q_m}{\Delta n} = -\frac{m\pi}{} \tag{6}$$

Therefore, the effect of roughness is more on higher m confined phonons (m close to n). Also, the SLs with small thickness will show a stronger dependence on the monolayer fluctuations of the layer thickness. Therefore, the low index confined phonons in SLs with large layer thickness are best suited to determine the phonon dispersion from Raman scattering in SLs.

4. INTERFACE OPTICAL PHONONS

Two types of interface modes (IF) can exist in the SLs composed of polar semiconductors. The first type, called microscopic interface modes occurs due to the dissimilarity in the short-range interactions of the two constituent bulk materials in the SL. Such IF modes can only be obtained in a microscopic model and can exist even in SLs made of non-polar materials, for example, *Si-Ge* SL. The second type, called macroscopic IF modes, originates from the difference in the dynamic dielectric function $\varepsilon(\omega)$ of the two layer materials and are caused by the mismatch of macroscopic polarisation fields on either side of the interface[14,15]. Such modes occur only in polar semiconductor SLs. Only the macroscopic IF modes which were observed for the first time by Raman scattering in *GaAs-AlAs* SLs[13] are discussed here.

Neglecting retardation, the electric potential caused by the interface vibrations satisfies

$$\nabla^2 \phi\,(x, z) = 0 \tag{7}$$

The solution of Eqn. (7) with the boundary condition of continuity of electric field component E_x and electric displacement component D_z gives the dispersion relation for the interface modes[14, 15].

$$\cos(qd) = \cosh(k_x d_1)\cosh(k_x d_2) + 1/2\left(\eta + \frac{1}{\eta}\right)\sinh(k_x d_1)\sinh(k_x d_2) \tag{8}$$

where

$$\eta = \varepsilon_1(\omega)/\varepsilon_2(\omega) \tag{9}$$

Eqn. (8) is similar to Eqn. (1) with the replacement of K by η and $k_{1(2)}$ by k_x. Taking

$$\varepsilon_{1(2)}(\omega) = \varepsilon^{\infty}_{1,2}\,\frac{(\omega^2 - L^2_{1,2})}{(\omega^2 - T^2_{1,2})}$$

where $L(T)$ indicates LO (TO) phonon frequency in *GaAs* and *AlAs* layers. Using Eqns. (8)-(10), the dispersion curves are plotted in Fig. 7 for *GaAs-AlAs* SLs. The modes have symmetric (+ve sign) or antisymmetric (−ve sign) potential with respect to the centre of the layer.

In order to see the connection between the IF modes and the bulk confined modes with

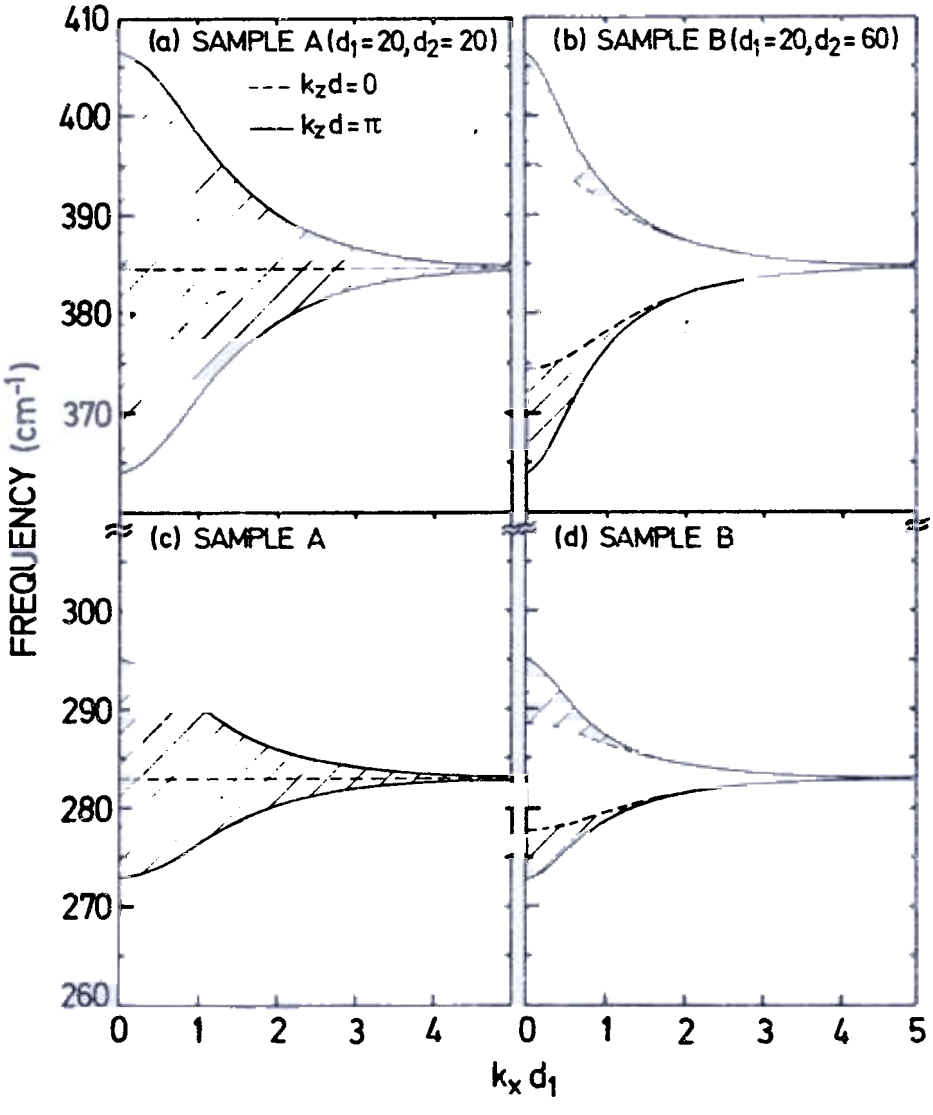

Figure 7. Calculated dispersion curves for the IF modes using Eqns. (8)-(10) for *GaAs-AlAs* SLs.

wave vector parallel to the interface, we take the limit $q \to 0$ and $k_x \to 0$ in Eqn. (8) to get

$$\varepsilon_1 d_2 + \varepsilon_2 d_1 = 0 \text{ or } <1/\varepsilon> \quad 0 \tag{11}$$

$$\varepsilon_1 d_1 + \varepsilon_2 d_2 = 0 \text{ or } <\varepsilon> \quad 0 \tag{12}$$

The Eqns. (11) and (12) are identical to those equations defining the bulk modes of a layered medium[36].

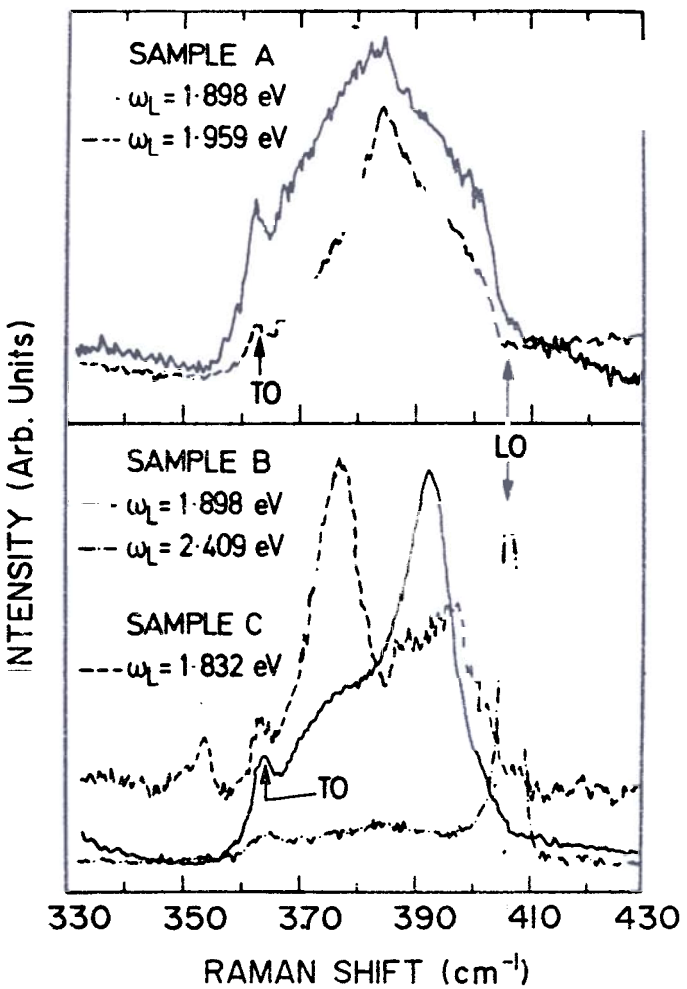

Figure 8. *AlAs*-like IF modes for three *GaAs-AlAs* SLs in $z(xx)z$ geometry (after Ref. 13).

Figure 8 shows backscattering Raman spectra for *AlAs*-like IF modes for the three *GaAs-AlAs* SLs. Samples *A*, *B* and *C* have *GaAs/AlAs* thicknesses (in Å) 20/20, 20/60 and 60/20, respectively[13]. Though in backscattering geometry $k_x = 0$, defects like interface roughness result in $k_x \neq 0$. Recently, the wave vector k_x dependence of the interface phonon-polaritons in a *GaAs-AlAs* heterostructure was studied by changing the angle of incidence[37] in Raman experiments. The analysis was done by incorporating retardation effects, which produce polariton modes and were neglected in Eqn. (8). The dependence of the IF mode frequency on q, as shown in Eqn. (8), has been investigated[36] $GaAs\text{-}Al_xGa_{1-x}As$ SLs by varying λ (compare Eqn. 2). In $Cd_{1-x}Mn_xTe/Cd_{1-y}Mn_yTe$ SLs grown on (111) face, interface phonons are shown to be selectively favoured in Raman scattering by the intermediate states associated with excitons localised at the interfaces[20]. Another interesting result has been an enormous enhancement of Raman intensities of the IF as well as the confined *LO* modes by the application of magnetic field perpendicular to the

layers[39]. This has been understood in terms of a scattering process involving phonon creation along with intra-Landau level photocarrier excitations which lead to scattering of photons with arbitrary $\vec{k}$.

A more complete continuum model for long-wavelength phonons in heterostructure has been constructed using an envelope-function formalism[40]. The effects of interfaces are taken into account in the form of boundary conditions written as linear relations among envelopes and their derivatives on both sides of the interface. The boundary conditions depend on the materials and the atomic configurations on the interface. What is interesting is that in certain cases, there are other boundary conditions in addition to the usual ones used in deriving Eqn. (8). It would be interesting to examine the effect of these new boundary conditions on the phonons.

Recently microscopic lattice dynamic models have been studied in which optical phonon modes with a finite wave vector parallel to the interface are dealt with[11, 12, 41, 42]. The interface modes calculated from the dielectric continuum model agree with the microscopic model which ignores the dispersion of the bulk *LO* and *TO* phonons. A realistic finite phonon dispersion in the microscopic model results in partial intermixing of the IF modes into bulk-like confined modes with nearby frequencies[41,42]. The affected small number of bulk-like modes due to intermixing are no longer confined to one layer.

5. EFFECT OF INTERFACE BROADENING AND ROUGHNESS

How Raman scattering has been shown to be a powerful technique to characterise the structural quality of the SLs, particularly the interface broadening and roughness is discussed in this section. We may recall that the acoustic and optical phonons have different spatial extent in the SL and hence would provide two different probes of the SL quality. The propogating acoustic phonons are sensitive to the periodicity d of the SL whereas the confined optical phonons are sensitive to the width and shape of the layers. The interface broadening has also been shown to affect the intensities of the folded LA phonons[6]. This has been understood by noting that the intensities of the folded acoustic phonons are related to the Fourier transform of modulation of the photoelastic tensor along the SL. The Fourier components for abrupt interfaces slowly decrease with increasing order m, whereas for a graded profile like a sinusoidal one, the zero order component only survives[6]. By taking 'erf profile' for the interfaces, ECM has been used to estimate the interface width parameter.

The frequencies of the confined LO_m modes, $\omega(LO_m)$ has been used to obtain information on the shape of the phonon quantum well[4,6,7]. For abrupt interfaces, the well will be square and the phonon energy levels will be proportional to m^2 (infinite square well approximation). For graded interfaces, the shape approximates to a parabola and the phonon energy levels will be proportional to m and hence will be equally spaced. Jusserand *et al.*[6] defined a shape parameter:

$$S = \frac{\omega(LO_5) - \omega(LO_3)}{\omega(LO_3) \quad \omega(LO_1)}$$

The parameter S for a perfect SL is 2.0 and it reduces to 1.0 in the parabolic-well limit. A quantitative estimate of the interface width has been made by using the linear chain model for the optic phonons[6].

Fasol *et al.*[5] have studied in detail the effect of interface roughness on the confined *LO* phonons by measuring Raman scattering from the SLs grown by different growth tech-

niques. As mentioned in section 3, these authors note that the higher order confined phonons are affected more than the lower order ones. By comparing the intensity of higher order phonons with the lower m phonons, it has been suggested[5] that the phonons parallel to the wells may be localised due to interface disorder, similar to Anderson localisation of electrons.

6. CONCLUSION

The novel features of phonons in the semiconductor SLs have been studied by Raman scattering and analysed in terms of continuum and microscopic models. It has been demonstrated that Raman scattering from the phonons can be used very effectively to characterise the structural qualities of the SLs. It is hoped that a complete quantitative understanding of the vibrational properties of the SLs will lead to better heterostructure devices.

REFERENCES

1. Klein, M.V., *IEEE J. Quantum Electronics*, **QE-22** (1986), 1760-1770.
2. Worlock, J.M., *In* Proc. Second International Conference on Phonon Physics, J. Kollar, N. Kroo, N. Menyhard & T. Siklos (Eds.), (World Scientific, Singapore) 1985, pp. 506-515.
3. Sood, A.K., *In* Vibrational Spectra and Structure, Vol. 17A, H.D. Bist, J.R. Durig & J.F. Sullivan (Eds.), (Elsevier, Amsterdam), 1989, pp. 295-322.
4. Wicks, G.W., Bradshaw, J.T. & Radulescu, D.C., *Appl. Phys. Lett.*, **52** (1988), 570-572.
5. Fasol, G., Tanaka, M., Sasaki, H. & Horikoshi, Y., *Phys. Rev.*, **B38** (1988), 6056-6065.
6. Jusserand, B., Alexandre, F., Paquet, D. & Roux, G. Le, *Appl. Phys. Lett.*, **47** (1985), 301-303.
7. Levi, D., Zhang Shu-Lin, Klein, M.V., Klem, J. & Morkoc, H., *Phys. Rev.*, **B36** (1987), 8032-8045.
8. Sood, A.K., Menendez, J., Cardona, M. & Ploog, K., *Phys. Rev. Lett.* **54** (1985), 2111-2114.
9. Jusserand, B., Paquet, D. & Regreny, A., *Phys. Rev.*, **B30** (1984), 6245-6247.
10. Colvard, C., Grant, T.A., Klein, M.V., Merlin, R., Fisher, R., Morkoc, H. & Gossard, A.C., *Phys. Rev.*, **B31** (1985), 2080-2091.
11. Ren Shang-Fen, Chu, H. & Chung, Y., *Phys. Rev. Lett.*, **59** (1987), 1841-1844; *Phys. Rev.*, **B37** (1988), 8899-8911.
12. Richter, E. & Strauch, D., *Solid State Communc.*, **64** (1987), 867-870.
13. Sood, A.K., Menendez, J., Cardona, M & Ploog, K., *Phys. Rev. Lett.*, **54** (1985), 2115-2118.
14. Pokatilov, E.P. & Berlin, S.I., *Phys. Stat. Solidi*, **B110** (1982), K75-K78; **B118** (1983), 567-573.
15. Camley, R.E. & Mills, D.L., *Phys. Rev.*, **B29** (1984), 1695-1706.
16. Santos, P.V., Sood, A.K., Cardona, M., Ploog, K., Ohmori Y. & Okamoto H.O., *Phys. Rev.*, **B37** (1988), 6381-6392.

17. Schwartz, G.P., Gualtieri, G.J., Sundar, W.A. & Farrow, L.A., *Phys. Rev.*, **B36** (1987), 4868-4877.

18. Ospelt, M., Bacsa, W., Henz, J., Mader, K.A. & Von Kanel, H., *Superlattices and Microstructures*, **5** (1989), 71-77.

19. Friess, E., Brugger, H., Eberl, K., Krotz, G. Abstreiter, *Solid State Communc.*, **69** (1989), 899-903.

20. Suh, E.K., Bartholomew, D.V., Ramdas, A.K., Rodriguez, S., Venugopalan, S., Kolodziejski, L.A. & Gunshor, R.L., *Phys. Rev.*, **B36** (1987), 4316-4328.

21. Santos, P., Hundhausen, M. & Ley, L., *Phys. Rev.*, **B33** (1986), 1516-1518; Santos, P., Ley, L., Mebert, J. & Koblinger, O., *Phys. Rev.*, **B36** (1987), 4858-4867.

22. Colvard, C., Merlin, R., Klein, M.V. & Gossard, A.C., *Phys. Rev. Lett.*, **45** (1980), 298-301.

23. Narayanamurthy, V., Störmer, H.L., Chin, M.A., Gossard, A.C. & Wiegmann, W., *Phys. Rev. Lett.*, **43** (1979), 2012-2015.

24. Rytov, S.M., *Sov. Phys. Acoust.*, **2** (1956), 68-70.

25. Jusserand, B., Alexandre, F., Dubard, J. & Paquet, D., *Phys. Rev.*, **B33** (1986), 2897-2899.

26. Barker, A.S. Jr., Merz, J.L. & Gossard, A.C., *Phys. Rev.* **B17** (1978), 3181-3196.

27. Sapriel, J., Michel, J.C., Toledano, J.C., Vacher, R., Kervarec, J. & Regreny, A., *Phys. Rev.*, **B28** (1983), 2007-2016.

28. Molinari, E., Fasolino, A. & Kunc, K., *Phys. Rev. Lett.*, **56** (1986), 1751.

29. Jusserand, B. & Paquet, D., *Phys. Rev. Lett.*, **56** (1986), 1752.

30. Sood, A.K., Menendez, J., Cardona, M. and Ploog, K., *Phys. Rev. Lett.*, **56** (1986), 1753.

31. Grant, T.A., Delaney, M., Klein, M.V., Houdre & Morkoc, H., *Phys. Rev.*, **B39** (1989), 1696-1702; Sela, I., Beserman, R. & Morkoc, H., *Phys. Rev.*, **B39** (1989), 3254-3257.

32. Ishibashi, A., Itabashi, M., Mori, Y, Kaneko, K., Kawado, S. & Watanabe, N., *Phys. Rev.*, **B33** (1986), 2887-2889.

33. Dolling, G. & Waugh, J.L.T., *In* Lattice Dynamics, R.F. Wallis Ed. (Pergamon, London) 1965, pp. 19-22.

34. Kustagi, K.C. & Weber, W., *Solid State Communc.* **18** (1976), 673-675.

35. Wang, Z.P., Jiang, D.S. & Ploog, K, *Solid State Communc.*, **65** (1988), 661-663.

36. Merlin, R., Colvard, C., Klein, M.V., Morkoc, H., Cho, A.Y. & Gossard, A.C., *Appl. Phys. Lett.*, **36** (1980), 43-45.

37. Nakayama, M., Ishida, M. & Sano, N., *Phys. Rev.*, **B38** (1988), 6348-635

38 Arora, A.K., Ramdas, A.K., Melloch, M.R. & Otsuka, N., *Phys. Rev.*, B36 1987 1021-1024.

39. Gammon, D., Merlin, R. & Morkoc, H., *Phys. Rev.*, **B35** (1987), 2552-2555.

40. Akera, H. & Ando, T., Preprint submitted to *Phys. Rev.*, **B** (1989), (to be published).

41. Huang, K., & Zhu, Bang-Fen, *Phys. Rev.*, **B38** (1988), 2183-2186; *Phys. Rev.*, **B38** (1988), 13377-13386.

42. Zhu, B., *Phys. Rev.*, **B38** (1988), 7694-7701.